THE JOURNAL OF PHYSICAL CHEMISTRY B
A JOURNAL OF THE AMERICAN CHEMICAL SOCIETY

pubs.acs.org/JPCB

Article

Thermodynamic Investigation of the Effect of Electric Field on Solid−Liquid Equilibrium

Sima Hejazi, Hassan Pahlavanzadeh, and Janet A. W. Elliott*

Cite This: J. Phys. Chem. B 2021, 125, 1271−1281

Read Online

ACCESS | Metrics & More | Article Recommendations

ABSTRACT: In this study, the thermal, mechanical, and chemical equilibrium conditions are derived for binary solid−liquid equilibrium under the effect of an electric field. As an example, the effect of an electric field on the water/glycerol solid−liquid phase diagram is computed over the complete mole fraction range. We show that the application of an electric field can affect the composition dependent freezing and precipitating processes, changing freezing and precipitating temperatures and changing the eutectic point temperature and mole fraction.

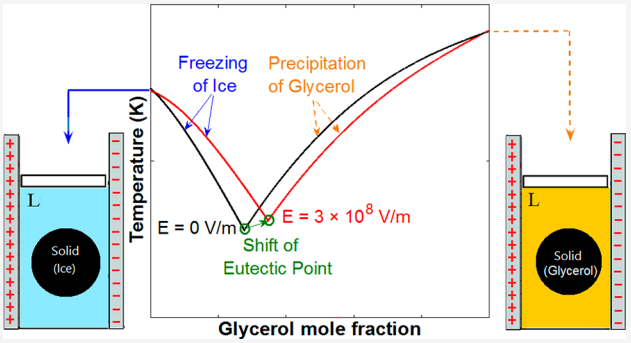

1. INTRODUCTION

Crystallization is widely used in different industrial applications, including the production of a wide range of materials as well as in the mineral processing industries and treatment of waste effluents.[1] The crystallization process can be divided into two main stages: nucleation and growth.[2] Nucleation is the formation of a new crystal at a high level of supersaturation. The radii of the nuclei must be large enough to overcome the free energy barrier so that growth can occur.[2]

Some experimental studies suggest that the application of direct current (DC) voltage promotes water crystallization with charge flow and static electric field,[3−16] while others find that particular fields can inhibit freezing or have no effect.[17−19] Charge flow, besides changing chemical potentials, causes several other phenomena during the growth process.[20] It has been shown that charge flow can substantially modify the supercooling of the melt by Peltier thermoelectric cooling[21] or, in contrast, by Joule heating,[21−23] therefore altering the driving force for crystal growth. Also, charge flow induces electromigration[21] that causes a Lorenz force[22,23] promoting mass transfer which can affect the crystal growth rate. By considering a static electric field, there are no currents or varying voltages.[24]

Interestingly, an electric field can act macroscopically and change the thermodynamic equations governing equilibrium and modify the solute transport and growth kinetics of the solid−liquid interface.[25,26] Quan et al. noted that for crystallization under the effect of an electric field an additional term (φ) must be added to the Gibbs free energy (G)[27]

$$\text{augmented free energy} = G + \varphi = U - TS + PV + \varepsilon' E^2 V \quad (1)$$

where U, T, S, P, ε', E, and V are internal energy, temperature, entropy, pressure, dielectric permittivity at the given electric field strength, electric field strength, and volume, respectively.

Jha et al.[28] reviewed the effect of DC voltage on the ice crystallization in food processes. Acharya and Bahadur[29] reviewed experimental studies on ice nucleation under the effect of DC and alternating current (AC) electric fields. Overall, they concluded that using an electric field can enhance ice nucleation significantly. Pahlavanzadeh et al.[30] experimentally studied the effect of a static electric field and a pulsed electric field on tetrahydrofuran hydrate nucleation temperature and growth time. It was observed that the static electric field could increase the nucleation temperature and growth time. They found that changing the static electric field to a pulsed electric field at an equal voltage, resulting in decreased electric field effectiveness.

In this work we use Gibbsian composite-system thermodynamics to derive the effect of an electric field on solid−liquid phase equilibrium. Gibbsian composite-system thermodynamics can be used to determine the equations for thermal, chemical, and mechanical equilibrium of a composite system

Received: September 25, 2020
Revised: December 30, 2020
Published: January 26, 2021

https://dx.doi.org/10.1021/acs.jpcb.0c08754
J. Phys. Chem. B 2021, 125, 1271−1281

by extremizing the entropy. Shardt and Elliott applied Gibbsian composite-system thermodynamics to derive the equilibrium conditions for the wetting of rough surfaces resulting in a line-fraction form of the Cassie–Baxter equation[31] and a new line-roughness-controlled Wenzel equation.[32] Gibbsian composite-system thermodynamics has been used to study the nucleation and thermodynamic stability of new fluid phase (liquid or vapor) formation at solid surfaces in several geometries,[33−35] including a thermodynamic description of surface nanobubbles.[36] Eslami and Elliott used Gibbsian composite-system thermodynamics to show why nucleation at a fluid surface occurs more readily than at a rigid surface.[37] Eslami and Elliott applied Gibbsian composite-system thermodynamics to the study of micro- and nanodrop liquid–liquid equilibrium,[38−40] including the role of a precipitating solute.[40] Elliott and Voitcu used Gibbsian composite-system thermodynamics to derive the conditions for equilibrium of a sessile drop in a gravitational field.[41] Through the framework of Gibbsian thermodynamics, extensive theoretical analyses have been carried out for investigating the effect of curved interfaces on liquid–vapor[42,43] and solid–liquid phase diagrams.[44−47] Liu et al.[47] applied Gibbsian thermodynamics to describe the impact of nanoscale interface curvature on binary solid–liquid equilibrium across the complete composition range of the phase diagram. They derived equations for the impact of solid–liquid interface curvature on the freezing liquidus and precipitating liquidus, and they showed that the eutectic point temperature and mole fraction are affected by interface curvature when compared with the traditional phase diagram. The effects were explored quantitatively for the glycerol/water binary system.

In this paper, we follow a similar approach to that of Liu et al.[47] to investigate the impact of an electric field (rather than curved interfaces) on the solid–liquid phase diagram across the complete composition range. Herein, we start by deriving the general conditions for solid–liquid equilibrium under the effect of an electric field. The conditions for equilibrium are used to quantify the effect of the electric field on the two liquidus lines and the eutectic point of the glycerol/water system.

2. THEORY

2.1. Thermodynamics of Electric Field. Using the general relation of electrostatics, the expression for the electric work (l_e) may be written as the energy given to the dielectric[48,49]

$$l_e = \frac{1}{2}\int_{V'} E D'\, \mathrm{d}V' \tag{2}$$

where

$$D' = \varepsilon_0 E + \mathcal{P}' \tag{3}$$

and thus

$$l_e = \frac{1}{2}\int_{V'} E\varepsilon_0 E\, \mathrm{d}V' + \frac{1}{2}\int_{V'} E\mathcal{P}'\, \mathrm{d}V' \tag{4}$$

or

$$\mathrm{d}l_e = \frac{\varepsilon_0 E^2}{2}\,\mathrm{d}V' + \frac{E\mathcal{P}'}{2}\,\mathrm{d}V' \tag{5}$$

where D' is the electric induction in the presence of an electric field, ε_0 is the electric permittivity of vacuum, E is the intensity of the electric field, $\mathcal{P}'$ is the total polarization in the presence of the electric field, and V' is the total volume under the effect of the electric field. The first term on the right-hand side of eq 4 is the energy for the field inside the total volume, and the second term is the work to polarize the dielectric. Also, for a simple system with m components the total polarization is defined as[48,49]

$$\mathcal{P}' = \sum_{i=1}^{m} x_i \mathcal{P}'_i \tag{6}$$

where x_i and $\mathcal{P}'_i$ are the mole fraction and the polarization of component i at the given electric field strength. $\mathcal{P}'_i$ can be calculated as[48,49]

$$\mathcal{P}'_i = \varepsilon_0(\varepsilon'_i - 1)E \tag{7}$$

Because ε'_i, the relative permittivity of component i in the electric field, and E have different values for different phases, the polarizability of molecules ($\mathcal{P}'_i$) is different for different phases (solid, liquid, or solid–liquid interface).

Equation 5 can be written for each bulk phase α as

$$\begin{aligned}\mathrm{d}l_e^{\alpha} &= \frac{\varepsilon_0 E^{\alpha 2}}{2}\,\mathrm{d}V'^{\alpha} + \sum_{i=1}^{m}\frac{E^{\alpha}}{2}\frac{n_i^{\alpha}\mathcal{P}'^{\alpha}_i}{n_T^{\alpha}}\,\mathrm{d}V'^{\alpha} \\ &= \frac{\varepsilon_0 E^{\alpha 2}}{2}\,\mathrm{d}V'^{\alpha} + \sum_{i=1}^{m}\frac{E^{\alpha}\mathcal{P}'^{\alpha}_i}{2n_T^{\alpha}}\,\mathrm{d}N'^{\alpha}_i\end{aligned} \tag{8}$$

where n_i^{α} is the number of moles of component i in phase α per unit volume of phase α, n_T^{α} is the total number of moles in phase α per unit volume of phase α, and N'^{α}_i is the number of moles of component i in phase α under the influence of the electric field.

Equation 5 can be written for each surface phase $\alpha\beta$ as

$$\mathrm{d}l_e^{\alpha\beta} = \sum_{i=1}^{m}\frac{E^{\alpha\beta}\mathcal{P}'^{\alpha\beta}_i}{2n_T^{\alpha\beta}}\,\mathrm{d}N'^{\alpha\beta}_i \tag{9}$$

For the thermodynamic study of electric systems there are many methods, depending on the choice of the fundamental variables. We shall discuss, for simplicity, only the case where the simple-system subsystems of a composite electric system (i.e., the separate phases) are each homogeneous.

For a simple bulk system with m components, the entropy differential can be written as in eq 10 using the fundamental relations and the definitions of intensive properties temperature (T), pressure (P), and chemical potential (μ)[50]

$$\mathrm{d}S = \frac{\mathrm{d}U}{T} + \frac{P}{T}\,\mathrm{d}V - \sum_{i=1}^{m}\frac{\mu_i}{T}\,\mathrm{d}N_i \tag{10}$$

where N_i is the number of moles of component i. Throughout this paper, the prime symbol on a variable indicates that the variable is evaluated under the impact of an electric field. Thus, eq 10 can be rewritten for phase α under the effect of an electric field as

$$\mathrm{d}S'^{\alpha} = \frac{\mathrm{d}U'^{\alpha}}{T'^{\alpha}} + \frac{P'^{\alpha}}{T'^{\alpha}}\,\mathrm{d}V'^{\alpha} - \sum_{i=1}^{m}\frac{\mu'^{\alpha}_i}{T'^{\alpha}}\,\mathrm{d}N'^{\alpha}_i \tag{11}$$

Similarly, the differential of the interface entropy under the influence of electric field is given by[51]

https://dx.doi.org/10.1021/acs.jpcb.0c08754
J. Phys. Chem. B 2021, 125, 1271−1281

$$dS'^{\alpha\beta} = \frac{dU'^{\alpha\beta}}{T'^{\alpha\beta}} - \frac{\sigma'^{\alpha\beta}}{T'^{\alpha\beta}} dA'^{\alpha\beta} - \sum_{i=1}^{m} \frac{\mu'^{\alpha\beta}_i}{T'^{\alpha\beta}} dN'^{\alpha\beta}_i \quad (12)$$

where $A'^{\alpha\beta}$ is the area of the interface and $\sigma'^{\alpha\beta}$ represents the solid−liquid interfacial tension under the effect of an electric field.

2.2. Derivation of General Conditions for Solid−Liquid Equilibrium under the Effect of Electric Field. The equilibrium states of a composite system can be determined from Gibbsian thermodynamics. Our objective is to find the effect of electric field application on the solid−liquid equilibrium of a two-component aqueous system. Consider the system illustrated in Figure 1. This solid−liquid system with a curved interface that will be analyzed under the effect of an electric field is contained in a piston−cylinder device forming a closed system within a surrounding reservoir. The system may exchange volume and energy with the reservoir but does not exchange any mass with the reservoir. Therefore, the number of molecules of each component in the system is constant. We assume that the solid is pure component 1. Therefore, molecules of component 1 are present in the solid phase, the liquid phase, and the solid−liquid interface. Molecules of component 2 are present in the liquid phase and the solid−liquid interface; however, they are not present in the solid.

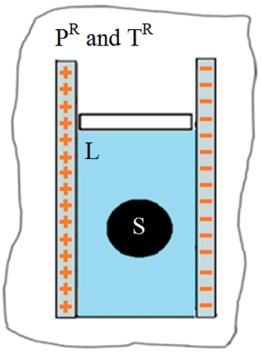

Figure 1. Schematic diagram of solid−liquid equilibrium in the presence of an electric field.

In this work, we develop the effect of an electric field on solid−liquid equilibrium. In this case, the piston−cylinder device imposes the pressure of the reservoir on the liquid phase. An equilibrium state occurs when the entropy of the composite system plus reservoir is at an extremum; mathematically, this means that

$$dS'^{S} + dS'^{L} + dS'^{SL} + dS^{R} = 0 \quad (13)$$

where superscripts "S" and "L" denote the solid and liquid phases, respectively, "SL" denotes the solid−liquid interface, and "R" denotes the reservoir surrounding the solid−liquid system. Based on eq 11, the differential entropy of the bulk liquid phase is given by the following equation:

$$dS'^{L} = \frac{dU'^{L}}{T'^{L}} + \frac{P'^{L}}{T'^{L}} dV'^{L} - \frac{\mu'^{L}_1}{T'^{L}} dN'^{L}_1 - \frac{\mu'^{L}_2}{T'^{L}} dN'^{L}_2 \quad (14)$$

Because component 2 does not exist in the solid phase, the differential of entropy of the solid phase (superscript "S") is written as

$$dS'^{S} = \frac{dU'^{S}}{T'^{S}} + \frac{P'^{S}}{T'^{S}} dV'^{S} - \frac{\mu'^{S}_1}{T'^{S}} dN'^{S}_1 \quad (15)$$

Using the Gibbs Surface of Tension approach, the curved solid−liquid interface (superscript "SL") is treated as a phase that has area but no volume and to which are assigned excess properties and an interfacial tension σ, the value for which does not depend explicitly on curvature. Therefore, the differential of the solid−liquid interface entropy is given by

$$dS'^{SL} = \frac{dU'^{SL}}{T'^{SL}} - \frac{\sigma'^{SL}}{T'^{SL}} dA'^{SL} - \frac{\mu'^{SL}_1}{T'^{SL}} dN'^{SL}_1 - \frac{\mu'^{SL}_2}{T'^{SL}} dN'^{SL}_2 \quad (16)$$

where A'^{SL} is the area of the interface, σ'^{SL} represents the solid−liquid interfacial tension, and μ'^{SL}_1 and μ'^{SL}_2 represent the chemical potentials of surface excess molecules of components 1 and 2 after electric field application. Finally, the differential of the entropy of the reservoir (superscript "R") may be written

$$dS^{R} = \frac{dU^{R}}{T^{R}} + \frac{P^{R}}{T^{R}} dV^{R} - \sum_{j=1}^{m} \frac{\mu^{R}}{T^{R}} dN^{R}_j \quad (17)$$

It is considered that the reservoir is not under the influence of the electric field.

For spontaneous changes about equilibrium, the total internal energy of the system plus reservoir plus electric work is constant:

$$dU^{R} = -dU'^{S} - dl^{S}_e - dU'^{L} - dl^{L}_e - dU'^{SL} - dl^{SL}_e \quad (18)$$

where

$$dl^{S}_e = \frac{\varepsilon_0 (E^{S})^2}{2} dV'^{S} + \sum_{i=1}^{m} \frac{E^{S} \mathcal{P}'^{S}_i}{2 n^{S}_T} dN'^{S}_i \quad (19)$$

and

$$dl^{L}_e = \frac{\varepsilon_0 (E^{L})^2}{2} dV'^{L} + \sum_{i=1}^{m} \frac{E^{L} \mathcal{P}'^{L}_i}{2 n^{L}_T} dN'^{L}_i \quad (20)$$

and

$$dl^{SL}_e = \sum_{i=1}^{m} \frac{E^{SL} \mathcal{P}'^{SL}_i}{2 n^{SL}_T} dN'^{SL}_i \quad (21)$$

The total volume of the system plus reservoir is constant:

$$dV^{R} = -dV'^{S} - dV'^{L} \quad (22)$$

The total number of moles of component 1 in the system (in the solid phase, liquid phase, and solid−liquid interface) is constant:

$$dN'^{S}_1 = -dN'^{L}_1 - dN'^{SL}_1 \quad (23)$$

The total number of moles of component 2 in the system (in the liquid phase and solid−liquid interface) is constant:

$$dN'^{L}_2 = -dN'^{SL}_2 \quad (24)$$

The number of moles of each species in the reservoir is constant:

$$dN^{R}_j = 0 \quad (25)$$

https://dx.doi.org/10.1021/acs.jpcb.0c08754
J. Phys. Chem. B 2021, 125, 1271−1281

The next step is to use geometric knowledge to impose relationships between phase volumes and area because changes in these are not independent. For a spherical solid nucleus, the following relationships hold for differential area and volume:[52]

$$dA'^{SL} = 8\pi r'^{S}\, dr'^{S} \tag{26}$$

$$dV'^{S} = 4\pi (r'^{S})^2\, dr'^{S} \tag{27}$$

where r'^{S} is the radius of the spherical solid nucleus after the application of the electric field.

Substituting eqs 14−27 into eq 13 and collecting like terms gives

$$\begin{aligned}
&\left(\frac{1}{T'^{S}} - \frac{1}{T^{R}}\right) dU'^{S} + \left(\frac{1}{T'^{L}} - \frac{1}{T^{R}}\right) dU'^{L} \\
&+ \left(\frac{1}{T'^{SL}} - \frac{1}{T^{R}}\right) dU'^{SL} \\
&+ \left(\frac{\mu_1'^{S} + \mathcal{P}_1'^{S}E^{S}/2n_T^{S}}{T'^{S}} - \frac{\mu_1'^{L} + \mathcal{P}_1'^{L}E^{L}/2n_T^{L}}{T'^{L}}\right) dN_1'^{L} \\
&+ \left(\frac{\mu_1'^{S} + \mathcal{P}_1'^{S}E^{S}/2n_T^{S}}{T'^{S}} - \frac{\mu_1'^{SL} + \mathcal{P}_1'^{SL}E^{SL}/n_T^{SL}}{T'^{SL}}\right) dN_1'^{SL} \\
&+ \left(\frac{\mu_2'^{L} + \mathcal{P}_2'^{L}E^{L}/2n_T^{L}}{T'^{l}} - \frac{\mu_2'^{SL} + \mathcal{P}_2'^{SL}E^{SL}/2n_T^{SL}}{T'^{SL}}\right) dN_2'^{SL} \\
&+ \left(\frac{P'^{L} - \frac{\varepsilon_0(E^{L})^2}{2}}{T'^{L}} - \frac{P^{R}}{T^{R}}\right) dV'^{L} \\
&+ \left[4\pi (r'^{S})^2 \left(\frac{P'^{S} - \frac{\varepsilon_0(E^{S})^2}{2}}{T'^{S}} - \frac{P^{R}}{T^{R}}\right) - \frac{\sigma'^{SL}}{T'^{SL}} 8\pi r'^{S}\right] dr'^{S} \\
&= 0
\end{aligned} \tag{28}$$

For eq 28 to be satisfied for all possible displacements from equilibrium, each of the coefficients multiplying the differentials must be equal to zero. When these coefficients are set to zero, the following conditions for equilibrium can be derived.

$$T'^{S} = T'^{L} = T'^{SL} = T^{R} \tag{29}$$

$$\mu_1'^{S} + \mathcal{P}_1'^{S}E^{S}/2n_T^{S} = \mu_1'^{L} + \mathcal{P}_1'^{L}E^{L}/2n_T^{L} \tag{30}$$

$$\mu_2'^{L} + \mathcal{P}_2'^{L}E^{L}/2n_T^{L} = \mu_2'^{SL} + \mathcal{P}_2'^{SL}E^{SL}/2n_T^{SL} \tag{31}$$

$$P'^{L} - \frac{\varepsilon_0(E^{L})^2}{2} = P^{R} \tag{32}$$

$$P'^{S} - P'^{L} = \frac{2\sigma'^{SL}}{r'^{S}} + \left(\frac{\varepsilon_0(E^{S})^2}{2} - \frac{\varepsilon_0(E^{L})^2}{2}\right) \tag{33}$$

In the absence of an electric field

$$P^{L} = P^{R} \tag{34}$$

Therefore, eq 32 can be written as

$$P'^{L} - P^{L} = \frac{\varepsilon_0(E^{L})^2}{2} \tag{35}$$

and eq 33 as

$$P'^{S} - P^{L} = \frac{2\sigma'^{SL}}{r'^{S}} + \frac{\varepsilon_0(E^{S})^2}{2} \tag{36}$$

where E^{L} and E^{S} represent the electric field strengths in the liquid and solid phases, respectively.

When the electric field strength between two charged plates is E^0, we can consider E^{L} and E^{S} as[53]

$$E^{L} = E^{0} \tag{37}$$

and

$$E^{S} = \left(\frac{3\varepsilon'^{L}}{\varepsilon'^{S} + 2\varepsilon'^{L}}\right) E^{0} \tag{38}$$

where ε'^{L} and ε'^{s} are the relative permittivities of the liquid and solid phases in the presence of the electric field, respectively.

Equation 29 is the thermal equilibrium condition. Equations 30 and 31 are electrochemical equilibrium conditions. Equation 32 is the condition for mechanical equilibrium between the reservoir and liquid phase. Equation 33 is the condition for mechanical equilibrium between the solid and liquid phases under the effect of an electric field; it is the familiar Young−Laplace equation modified for the effect of an electric field.

2.3. Solid−Liquid Equilibrium Temperature after the Application of Electric Field. We combine the thermal equilibrium (equality of temperature of the solid phase, liquid phase, and solid−liquid interface) in eq 29, and the equality of the electrochemical potentials of component 1 in the solid and liquid, eq 30, noting that the pressures in the solid and liquid will be different, to get

$$\begin{aligned}
&\mu_1'^{L}(T'_{m,1}, P'^{L}, x_1^{L}) + \mathcal{P}_1'^{L}E^{L}/2n_T^{L} \\
&\quad = \mu_1'^{S}(T'_{m,1}, P'^{S}) + \mathcal{P}_1'^{S}E^{S}/2n_T^{S}
\end{aligned} \tag{39}$$

where $T'_{m,1}$ is the solid−liquid equilibrium temperature at the pressure of the liquid phase under the influence of an electric field (P'^{L}). Equation 39 assumes that the solid is pure component 1 and the liquid phase mole fraction of component 1 is x_1^{L}.

To develop the governing equation for the phase diagram, equations of state for the chemical potentials must be inserted into eq 39. The chemical potential of the solidifying component in the pure solid phase can be found by assuming that the solid phase is incompressible and that the solid molar entropy is independent of temperature, and thus the chemical potential can be expressed by[50]

$$\begin{aligned}
\mu_1'^{S}(T'_{m,1}, P'^{S}) = \mu_1^{S}(T_{m,1}^{0}, P^{L}) - s_1^{S}(T'_{m,1} - T_{m,1}^{0}) \\
+ v_1^{S}(P'^{S} - P^{L})
\end{aligned} \tag{40}$$

The melting point of pure component 1 in the absence of an electric field ($T_{m,1}^{0}$) and the bulk phase pressure before electric field application, P^{L}, are chosen as the reference point for calculating the chemical potential. s_1^{S} and v_1^{S} are the molar entropy and molar volume of pure component 1 in the solid phase at the reference point, respectively. Substituting eq 36 into eq 40 gives

https://dx.doi.org/10.1021/acs.jpcb.0c08754
J. Phys. Chem. B 2021, 125, 1271−1281

$$\mu'^{S}_1(T'_{m,1}, P'^{S}) = \mu^{S}_1(T^0_{m,1}, P^L) - s^S_1(T'_{m,1} - T^0_{m,1}) + v^S_1\left(\frac{2\sigma'^{SL}}{r'^{S}}\right) + v^S_1\left(\frac{\varepsilon_0(E^S)^2}{2}\right) \quad (41)$$

For the chemical potential of component 1 in the liquid solution, we use

$$\mu'^{L}_1(T'_{m,1}, P'^{L}, x^L_1) = \mu^{L}_1(T^0_{m,1}, P^L) - s^L_1(T'_{m,1} - T^0_{m,1}) + RT'_{m,1}\ln(x^L_1\gamma^L_1) + v^L_1(P'^{L} - P^L) \quad (42)$$

where s^L_1 and v^L_1 are the molar entropy and molar volume of pure component 1 in the liquid phase at $T^0_{m,1}$ and P^L, respectively. γ^L_1 and x^L_1 are the activity coefficient and mole fraction of component 1 in the liquid phase. Substituting eq 35 into eq 42 gives

$$\mu'^{L}_1(T'_{m,1}, P'^{L}, x^L_1) = \mu^{L}_1(T^0_{m,1}, P^L) - s^L_1(T'_{m,1} - T^0_{m,1}) + RT'_{m,1}\ln(x^L_1\gamma^L_1) + v^L_1\left(\frac{\varepsilon_0(E^L)^2}{2}\right) \quad (43)$$

Substituting eqs 41 and 43 into eq 39, and replacing $s^L_1 - s^S_1$ using the thermodynamic identity

$$\frac{1}{s^L_1 - s^S_1} = \frac{T^0_{m,1}}{\Delta H^{fus}_1} \quad (44)$$

where ΔH^{fus}_1 is the molar enthalpy of fusion for pure component 1 at $T^0_{m,1}$ and P^L, leads to

$$\ln(x^L_1\gamma^L_1) = \frac{\Delta H^{fus}_1}{RT^0_{m,1}}\left(1 - \frac{T^0_{m,1}}{T'_{m,1}}\right) + \frac{v^S_1}{RT'_{m,1}}\left(\frac{2\sigma'^{SL}}{r'^{S}}\right) + \frac{v^S_1\varepsilon_0(E^S)^2 - v^L_1\varepsilon_0(E^L)^2}{2RT'_{m,1}} + \frac{(\mathcal{P}'^{S}_1E^S/n^S_T - \mathcal{P}'^{L}_1E^L/n^L_T)}{2RT'_{m,1}} \quad (45)$$

Rearranging eq 45 for the solid−liquid equilibrium temperature yields

$$T'_{m,1} = \frac{\frac{2v^S_1\sigma'^{SL}}{r'^{S}} - \Delta H^{fus}_1 + \frac{v^S_1\varepsilon_0(E^S)^2 - v^L_1\varepsilon_0(E^L)^2 + \mathcal{P}'^{S}_1E^S/n^S_T - \mathcal{P}'^{L}_1E^L/n^L_T}{2}}{R\ln(x^L_1\gamma^L_1) - \frac{\Delta H^{fus}_1}{T^0_{m,1}}} \quad (46)$$

Liu et al. derived the following relation for the solid−liquid equilibrium temperature under the effect of a curved surface:[47]

$$T_{m,1} = \frac{\frac{2v^S_1\sigma^{SL}}{r^s} - \Delta H^{fus}_1}{R\ln(x^L_1\gamma^L_1) - \frac{\Delta H^{fus}_1}{T^0_{m,1}}} \quad (47)$$

They showed that the solid−liquid phase diagram of the water/glycerol system does not change significantly as a function of the curvature when the radius of curvature is above 100 nm. If the solid nucleus is large enough (above 100 nm) that the effect of curvature on the solid−liquid equilibrium is negligible, we can study the effect of the electric field only. Therefore, the freezing or precipitating temperature change ($\Delta T'$) under the effect of an electric field can be calculated as

$$\Delta T' = T^0_{m,1} - T'_{m,1} = \frac{RT^0_{m,1}\ln(x^L_1\gamma^L_1) - \frac{v^S_1\varepsilon_0(E^S)^2 - v^L_1\varepsilon_0(E^L)^2 + \mathcal{P}'^{S}_1E^S/n^S_T - \mathcal{P}'^{L}_1E^L/n^L_T}{2}}{R\ln(x^L_1\gamma^L_1) - \frac{\Delta H^{fus}_1}{T^0_{m,1}}} \quad (48)$$

Equation 48 can be compared to eq 49 that has been derived by Liu et al. to investigate the freezing or precipitating temperature change (ΔT) under the impact of curvature.[47]

$$\Delta T = T^0_{m,1} - T_{m,1} = \frac{RT^0_{m,1}\ln(x^L_1\gamma^L_1) - \frac{2v^S_1\sigma^{SL}}{r^S}}{R\ln(x^L_1\gamma^L_1) - \frac{\Delta H^{fus}_1}{T^0_{m,1}}} \quad (49)$$

There have been many efforts to measure the dielectric constants of liquids confined in regions with nanometer scale dimensions.[54−57] Results indicate that liquid molecules in a confined space are highly oriented, which implies that the dielectric constant may be different from that in the bulk. For example, the dielectric constant of water in a 0.3 nm Stern layer (the first layer of the electric double layer at a surface) was found to be approximately 6,[58] and the dielectric constant of water in a 330 nm diffuse layer (the second layer of the electric double layer) was estimated to be approximately 12,[59] both of which are much lower than that of the bulk. Consequently, this leads to inhomogeneity of dielectric behavior near surfaces. On the other hand, Fumagalli et al.[60] proved that water confined in spaces with dimensions of more than 600 nm does not have very different dielectric behavior from bulk water. In this work, we assume that water and glycerol are confined in spaces larger than 600 nm and thus show dielectric behaviors similar to those in the bulk, and we consider homogeneous dielectric behavior.

3. RESULTS AND DISCUSSION

3.1. Dielectric Constants of Water and Glycerol at High Electric Field Strength in Liquid Phase. Debye was the first to attempt to derive a relation to calculate dielectric constants of polar dielectrics at high electric field strengths. At high field strengths, the saturation effect is of importance so that the effective polar dielectric constant would be less than the ordinary value. In fact, the individual dielectric molecules become highly oriented under a large electric field and the dielectric constants of polar dielectrics may significantly decrease as the electric field increases.[61−65]

Here, the Booth model[63−65] is used to account for the effects of the electric field on the dielectric constant. It is expressed as

$$\varepsilon'^{L}(E) = I^2 + (\varepsilon^L - I^2)\frac{3}{\beta E}\left(\coth(\beta E) - \frac{1}{\beta E}\right), \quad E > 10^7\ \mathrm{V/m}$$
$$\varepsilon'^{L} = \varepsilon^L, \quad E < 10^7\ \mathrm{V/m} \quad (50)$$

where E is the electric field strength, ε'^{L} is the relative permittivity at an electric field strength of E, I and ε^L are the index of refraction of the dielectric and the dielectric constant at zero electric field, and β is a constant for a particular polar dielectric. Using the Taylor series for coth(βE), eq 50 can be written as eq 51 for $E > 10^7$ V/m:

https://dx.doi.org/10.1021/acs.jpcb.0c08754
J. Phys. Chem. B 2021, 125, 1271−1281

$$\varepsilon'(E) = I^2 + (\varepsilon - I^2)\left(1 - \frac{\beta^2}{15}E^2\right) \tag{51}$$

In order to use eq 51 for glycerol, we need to calculate β for water (β_w) and then estimate β for glycerol (β_g).

The Kirkwood theory is applied in detail to water as[64]

$$\varepsilon'^{L}_{w}(E) = I_w^2 + \frac{14\bar{N}_w\pi\bar{\mu}_w^2(I_w^2+2)^2}{27kT} \times \left(1 - \frac{73\bar{\mu}_w^2(I_w^2+2)^2}{180k^2T^2}E^2\right) \tag{52}$$

where ε'^{L}_{w} is the dielectric constant of water under the influence of high electric field, $\bar{N}_w$ is the number of water molecules per unit volume, $\bar{\mu}_w$ is the dipole moment of water molecules in units of debye, I_w is the water refractive index, and T is considered to be 300 K. Comparing eq 52 with eq 51, we get relations for ε^{L}_{w} and β_w:

$$\varepsilon^{L}_{w} - I_w^2 = \frac{14\bar{N}_w\pi\bar{\mu}_w^2(I_w^2+2)^2}{27kT} \tag{53}$$

and

$$\beta_w^2 = \frac{15(73\bar{\mu}_w^2(I_w^2+2)^2)}{180k^2T^2} \tag{54}$$

which shows the following dependence on $\bar{\mu}_w$ and I_w:

$$\beta_w^2 \propto \bar{\mu}_w^2(I_w^2+2)^2 \tag{55}$$

We assume a similar dependence as in eq 55 applies for glycerol:

$$\beta_g^2 \propto \bar{\mu}_g^2(I_g^2+2)^2 \tag{56}$$

where $\bar{\mu}_g$ is the dipole moment of glycerol molecules and I_g is the glycerol refractive index. By dividing eq 55 by eq 56, we have

$$\frac{\beta_w^2}{\beta_g^2} = \frac{\bar{\mu}_w^2(I_w^2+2)^2}{\bar{\mu}_g^2(I_g^2+2)^2} \tag{57}$$

I_g and I_w can be calculated from the next formula:[66]

$$\mathrm{Rm} = \left(\frac{\mathrm{MW}}{\rho}\right)\left(\frac{I^2-1}{I^2+2}\right) \tag{58}$$

where Rm is the predicted molar refractivity and MW is the molar mass. Equation 58 can be written for glycerol and water as

$$\mathrm{Rm}_g = \left(\frac{\mathrm{MW}_g}{\rho_g^L}\right)\left(\frac{I_g^2-1}{I_g^2+2}\right) \tag{59}$$

$$\mathrm{Rm}_w = \left(\frac{\mathrm{MW}_w}{\rho_w^L}\right)\left(\frac{I_w^2-1}{I_w^2+2}\right) \tag{60}$$

where Rm_g and Rm_w are the predicted molar refractivities of glycerol and water and MW_g and MW_w are the molar masses of glycerol and water, respectively (see Table 1). Subscript "1" represents the solidifying component.

Table 1. Values of Molar Refractivities,[a] Molar Masses, and Densities of Glycerol and Water to Calculate Their Refractive Indexes

	Rm_1 (cm^3/mol)	MW_1 (g/mol)	ρ_1^S (g/cm^3) at $T^0_{m,1}$	ρ_1^L (g/cm^3) at $T^0_{m,1}$
glycerol	20.572	92.094	1.34	1.26
water	3.581	18	0.92	1

[a]Data from ref 67.

We can use Rm, MW, and ρ to acquire the predicted refractive indexes for glycerol and water based on eqs 59 and 60, respectively. Results are presented in Table 2.

Table 2. Values of Dielectric Constants at Zero Electric Field,[a] Dipole Moments,[b] and Calculated Refractive Indexes of Glycerol and Water in Liquid Phase

	ε_1^L	$\bar{\mu}_1$ (D)	I_1
glycerol	47.2	2.67	1.42
water	79.46	2.1	1.33

[a]Data from ref 53. [b]Data from ref 64.

The values of the dielectric constants of glycerol and water in the liquid phase and zero electric field are $\varepsilon_g^L = 47.2$ and $\varepsilon_w^L = 79.46$, respectively.[53] $\bar{\mu}_g$ and $\bar{\mu}_w$, which are the dipole moments of glycerol molecules and water molecules, equal 2.67 and 2.1 D, respectively.[64]

As a result, the relationship between β_w and β_g is calculated from eq 57 as

$$\frac{\beta_w}{\beta_g} = 0.54 \tag{61}$$

Then β_w can be calculated from eq 54 as $\beta_w = 0.91 \times 10^{-8}$ m/V and the value substituted into eq 61 resulting in $\beta_g = 1.68 \times 10^{-8}$ m/V. By substituting this value of β_g and the values in Table 2 into eq 51, the following equation is obtained for the dielectric constant of glycerol at high electric field strengths.

$$\varepsilon'^{L}_{g}(E) = 1.42^2 + (47.2 - 1.42^2)\left(1 - \frac{(1.68\times10^{-8})^2}{15}E^2\right) \tag{62}$$

Figure 2 shows the predicted variation of the dielectric constants of water and glycerol under the influence of high electric field.

3.2. Dielectric Constants of Water and Glycerol at High Electric Field Strength in Solid Phase. Equation 63 is used to solve for the change of dielectric constant of polar components when density changes at constant temperature.[68]

$$\rho^L\left(\frac{\partial\varepsilon'}{\partial\rho}\right)_T = \frac{\varepsilon'^{L}(\varepsilon'^{L}-1)(2\varepsilon'^{L}+4I^2(\varepsilon'^{L}+1)-I^4)}{3(2\varepsilon'^{L2}+I^4)} \tag{63}$$

where ε'^{L} and ρ^L are the dielectric constant in the presence of the electric field and the density of the polar component in the liquid phase. T is the temperature and I is the refractive index. Here, we use eq 63 to calculate the dielectric constants of glycerol and water in the solid phase (ε'^{S}_{g}, ε'^{S}_{w}), from their liquid dielectric constants:

https://dx.doi.org/10.1021/acs.jpcb.0c08754
J. Phys. Chem. B 2021, 125, 1271−1281

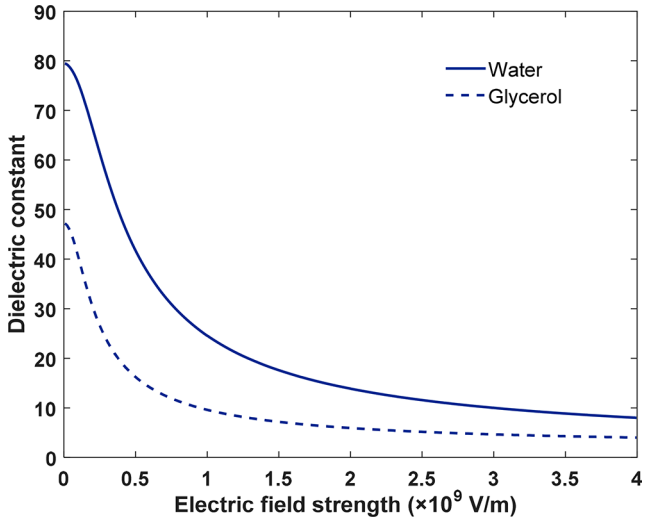

Figure 2. Water and glycerol dielectric constants versus electric field strength.

$$\rho_g^L\left(\frac{\varepsilon'^S_g - \varepsilon'^L_g}{\rho_g^S - \rho_g^L}\right)_T = \frac{\varepsilon'^L_g(\varepsilon'^L_g - 1)(2\varepsilon'^L_g + 4(I_g)^2(\varepsilon'^L_g + 1) - (I_g)^4)}{3(2(\varepsilon'^L_g)^2 + (I_g)^4)} \quad (64)$$

$$\rho_w^L\left(\frac{\varepsilon'^S_w - \varepsilon'^L_w}{\rho_w^S - \rho_w^L}\right)_T = \frac{\varepsilon'^L_w(\varepsilon'^L_w - 1)(2\varepsilon'^L_w + 4(I_w)^2(\varepsilon'^L_w + 1) - (I_w)^4)}{3(2(\varepsilon'^L_w)^2 + (I_w)^4)} \quad (65)$$

where ρ_g^S and ρ_g^L are the densities of glycerol in the solid phase and liquid phase, respectively, and ρ_w^S and ρ_w^L are the densities of water in the solid phase and liquid phase, respectively (see Table 1).

Therefore, we estimate the dielectric constants of glycerol and water in the solid phase at their melting point temperatures at high electric field strengths.

The dielectric constant values for three different electric field strengths of 10^8, 2×10^8, and 3×10^8 V/m for glycerol and water in liquid and solid phases are presented in Table 3.

Table 3. Dielectric Constants of Glycerol and Water in Solid Phase and Liquid Phase at High Electric Field Strengths

	$E = 10^8$ V/m	$E = 2 \times 10^8$ V/m	$E = 3 \times 10^8$ V/m
glycerol	$\varepsilon'^L_g = 40.48$	$\varepsilon'^L_g = 30.45$	$\varepsilon'^L_g = 23.58$
	$\varepsilon'^S_g = 44.98$	$\varepsilon'^S_g = 33.81$	$\varepsilon'^S_g = 26.16$
water	$\varepsilon'^L_w = 75.48$	$\varepsilon'^L_w = 66.37$	$\varepsilon'^L_w = 56.60$
	$\varepsilon'^S_g = 66.53$	$\varepsilon'^S_w = 58.50$	$\varepsilon'^S_w = 49.90$

3.3. Effect of Electric Field on the Solid–Liquid Equilibrium Phase Diagram and the Eutectic Point for the Water/Glycerol System.

Using eq 48 developed in section 2.3 for the solid–liquid equilibrium temperature under the effect of an electric field, we calculate the liquidus lines of the phase diagram for the glycerol/water system under the influence of an electric field and compare them to the traditional phase diagram. We use $T'_{m,P}$ and $T'_{m,F}$ to represent the precipitation temperature of glycerol and the freezing temperature of water, respectively, giving eqs 66 and 67:

$$T'_{m,P} = \frac{-\Delta H_g^{fus} + \frac{\nu_g^S\varepsilon_0(E^S)^2 - \nu_g^L\varepsilon_0(E^L)^2 + \mathcal{P}'^S_g E^S/n_T^S - \mathcal{P}'^L_g E^L/n_T^L}{2}}{R\ln(x_g^L\gamma_g^L) - \frac{\Delta H_g^{fus}}{T^0_{m,P}}} \quad (66)$$

$$T'_{m,F} = \frac{-\Delta H_w^{fus} + \frac{\nu_w^S\varepsilon_0(E^S)^2 - \nu_w^L\varepsilon_0(E^L)^2 + \mathcal{P}'^S_w E^S/n_T^S - \mathcal{P}'^L_w E^L/n_T^L}{2}}{R\ln((1 - x_g^L)\gamma_w^L) - \frac{\Delta H_w^{fus}}{T^0_{m,F}}} \quad (67)$$

where x_g^L and ν_g^L represent the mole fraction and molar volume of glycerol in the liquid phase. ν_g^S, ΔH_g^{fus}, and $T^0_{m,P}$ are the molar volume of pure glycerol solid and the molar enthalpy of fusion and melting point of pure glycerol, respectively, in the absence of an electric field in the precipitating process. ν_w^S and ν_w^L are the molar volumes of pure water in solid and liquid phases, respectively. ΔH_w^{fus} and $T^0_{m,F}$ are the molar enthalpy of fusion and melting point of pure water, respectively, in the absence of an electric field in the freezing process. Values for the mentioned parameters can be found in Table 4. Subscript "1" represents the solidifying component.

Table 4. Properties of Pure Water and Pure Glycerol at a Pressure of 1 atm[a]

	$T^0_{m,1}$ (K)	ΔH_1^{fus} (J/mol) at $T^0_{m,1}$	ν_1^S (m^3/mol) at $T^0_{m,1}$	ν_1^L (m^3/mol) at $T^0_{m,1}$
glycerol	291.35	18300	6.896×10^{-5}	7.3×10^{-5}
water	273.15	6010	1.963×10^{-5}	1.8×10^{-5}

[a]Data from ref 69.

The activity coefficients of glycerol and water in the liquid phase (γ_g^L and γ_w^L in eqs 66 and 67) were previously calculated by Liu et al.[47] They used the two-parameter Margules equation (eqs 68 and 69).

$$\ln(\gamma_g^L) = [A_{gw} + 2(A_{wg} - A_{gw})x_g^L](x_w^L)^2 \quad (68)$$

$$\ln(\gamma_w^L) = [A_{wg} + 2(A_{gw} - A_{wg})x_w^L](x_g^L)^2 \quad (69)$$

They found the values of the Margules coefficients by fitting eq 47 to the data measured by Lane[70] to get $A_{wg} = -1.0952$ and $A_{gw} = -2.1641$.

Equation 7 is used to calculate the polarizations of glycerol and water in the solid phase ($\mathcal{P}'^S_g$, $\mathcal{P}'^S_w$) and liquid phase ($\mathcal{P}'^L_g$, $\mathcal{P}'^L_w$) from the values of their dielectric constants (ε'^S_g, ε'^S_w, ε'^L_g, ε'^L_w).

Figure 3a shows the glycerol/water solid–liquid phase diagram in the absence of an electric field. It was produced with eq 47 based on Liu et al.'s paper[47] and according to Lane's data[70] when the radius of curvature is above 100 nm. As shown in Figure 3a, liquidus lines that show the freezing process (line A–Eu in Figure 3a) and the precipitating process (line Eu–B in Figure 3a) represent the onset of solidification of water and glycerol, respectively. Line A–Eu shows that the melting point of water depends on the composition of glycerol. Increasing the composition of glycerol results in decreasing the

https://dx.doi.org/10.1021/acs.jpcb.0c08754
J. Phys. Chem. B 2021, 125, 1271–1281

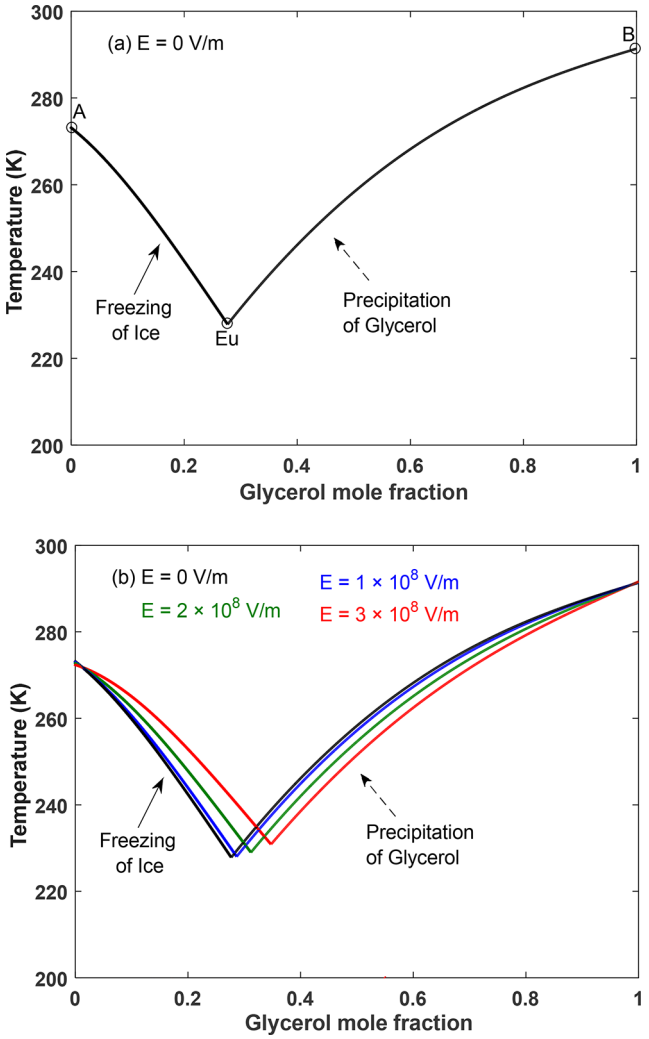

Figure 3. Temperature−composition phase diagram of solid−liquid equilibrium in a binary system at constant pressure (a) in the absence of electric field and (b) in the presence of electric field with strengths $E = 0$ V/m [black], $E = 10^8$ V/m [blue], $E = 2 \times 10^8$ V/m [green], and $E = 3 \times 10^8$ V/m [red].

melting point of water. Also, as line Eu−B shows, the precipitating point of glycerol decreases when the composition of water increases. The eutectic point (Eu) is the point where the two liquidus lines meet. At this point the solid of both water and glycerol and liquid coexist, and below the eutectic temperature no liquid can exist in the system at equilibrium.

Figure 3b shows the comparison between the water/glycerol solid−liquid phase diagram in the absence of an applied electric field and those under the application of different electric field strengths. According to Figure 3b, the application of an electric field causes an increase in the freezing point of water and a decrease in the solubility limit of glycerol. We can see that electric field strength of up to 10^8 V/m does not have an appreciable effect on the freezing and precipitating processes in comparison with those in the absence of an electric field. When the electric field strength increases up to 2×10^8 V/m, the freezing point increases and the solubility limit decreases, and the variation becomes larger when the electric field strength is enhanced further up to 3×10^8 V/m.

At the eutectic point, $T'_{m,F}$ equals $T'_{m,P}$ and equating eqs 66 and 67 yields eq 70 for the eutectic point solute mole fraction, x_g^{Eu}.

$$\frac{-\Delta H_g^{fus} + \frac{\nu_g^S \varepsilon_0 (E^S)^2 - \nu_g^L \varepsilon_0 (E^L)^2 + \mathcal{P}'^S_g E^S / n_T^S - \mathcal{P}'^S_g E^S / n_T^S}{2}}{R \ln(x_g^{Eu} \gamma_g^L) - \frac{\Delta H_g^{fus}}{T^0_{m,P}}} = \frac{-\Delta H_w^{fus} + \frac{\nu_w^S \varepsilon_0 (E^S)^2 - \nu_w^L \varepsilon_0 (E^L)^2 + \mathcal{P}'^S_w E^S / n_T^S - \mathcal{P}'^L_w E^L / n_T^L}{2}}{R \ln((1 - x_g^{Eu}) \gamma_w^L) - \frac{\Delta H_w^{fus}}{T^0_{m,F}}} \quad (70)$$

Equation 70 can be solved numerically together with eq 66 to yield the eutectic solute mole fraction and the eutectic temperature.

Figure 4 predicts how the eutectic point mole fraction changes with the electric field application in the range from 0

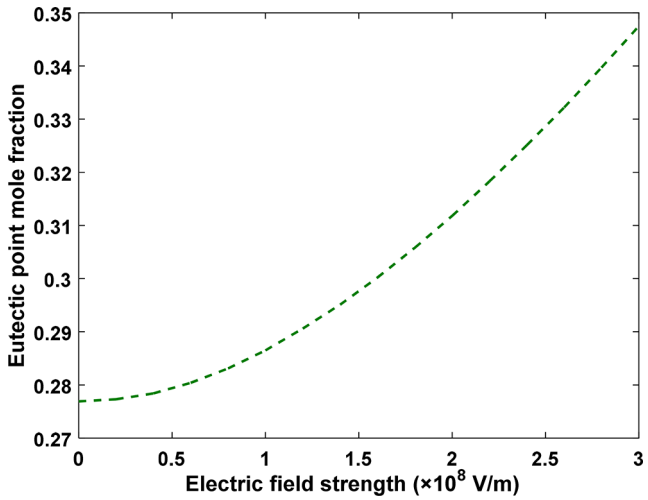

Figure 4. Predicted eutectic point mole fraction as a function of electric field strength.

to 3×10^8 V/m. In general, the eutectic point mole fraction increases as the electric field strength intensifies. To consider it more precisely, the eutectic point mole fraction stays almost the same when the electric field strength is under 10^8 V/m. When the electric field strength is above 10^8 V/m, the eutectic point mole fraction changes significantly so that the application of electric field with the strength of 3×10^8 V/m results in enhancing the eutectic point mole fraction up to 0.347.

Figure 5 shows the eutectic point temperature as a function of electric field strength in the range from 0 to 3×10^8 V/m. The eutectic point temperature of the water/glycerol system changes noticeably as the electric field strengthens. When the electric field strength increases up to 10^8 V/m, the eutectic point temperature does not have a significant change in comparison with its traditional value. By increasing the electric field strength up to 3×10^8 V/m, the eutectic point temperature increases up to 230.9 K.

4. CONCLUSION

By extremizing entropy subject to constraints, we have derived thermal, mechanical, and chemical equilibrium conditions for solid−liquid equilibrium in the presence of an electric field including the Young−Laplace equation modified for the effect

https://dx.doi.org/10.1021/acs.jpcb.0c08754
J. Phys. Chem. B 2021, 125, 1271−1281

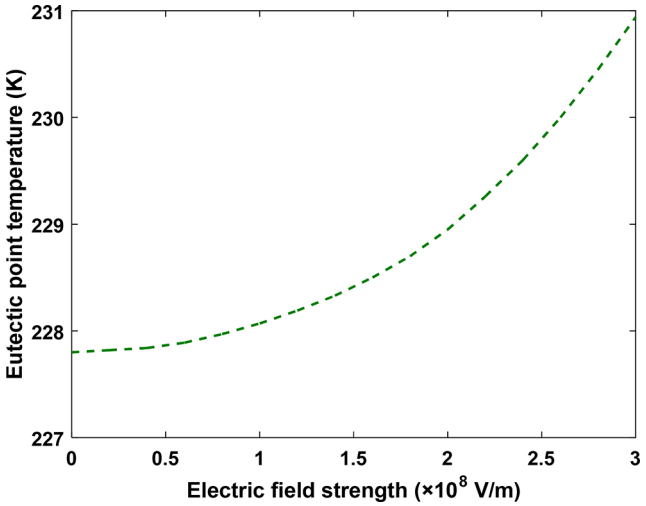

Figure 5. Predicted eutectic point temperature as a function of electric field strength.

of an electric field. The result is an equation that describes freezing point or precipitation from solution including the effects of mole fraction, interface curvature, and now electric fields. This equation can be considered an extension to the nonideal Gibbs–Thomson equation and nonideal Ostwald–Freundlich equations[47] to now include the effect of an applied electric field.

To illustrate the impact of the derived equations, we investigated the effect of an electric field on solid–liquid equilibrium for the water/glycerol system in the absence of interface curvature effects. According to the results, electric field affects both the freezing process and the precipitating process. Electric fields with strength of more than 10^8 V/m cause the freezing point of water to significantly increase and the solubility limit of glycerol to significantly decrease. Although the values of the eutectic point mole fraction and temperature are not affected noticeably under the influence of electric fields up to 10^8 V/m, increasing the strength of the electric field to more than 10^8 V/m increases them considerably. Electric fields of up to 0.8×10^8 V/m have been applied in solidification experiments, and electric field strengths of up to 3×10^{10} V/m have been investigated in simulations.[29] To apply the high electric field strengths at the nanoscale where both the curvature effects investigated by Liu et al.[47] and the electric effects investigated in this work would both come into play, the confinement dependency of dielectric constant and inhomogeneity in dielectric behavior occurring in 100 nm scale samples would need to be taken into account.[54−60]

AUTHOR INFORMATION

Corresponding Author

Janet A. W. Elliott − *Department of Chemical and Materials Engineering, University of Alberta, Edmonton, Alberta, Canada T6G 1H9;* orcid.org/0000-0002-7883-3243; Email: janet.elliott@ualberta.ca

Authors

Sima Hejazi − *Department of Chemical and Materials Engineering, University of Alberta, Edmonton, Alberta, Canada T6G 1H9; Faculty of Chemical Engineering, Tarbiat Modares University, Tehran 14115-336, Iran;* orcid.org/0000-0003-0337-1870

Hassan Pahlavanzadeh − *Faculty of Chemical Engineering, Tarbiat Modares University, Tehran 14115-336, Iran;* orcid.org/0000-0001-5203-3566

Complete contact information is available at: https://pubs.acs.org/10.1021/acs.jpcb.0c08754

Notes

The authors declare no competing financial interest.

ACKNOWLEDGMENTS

S. Hejazi carried out this work while a visiting Ph.D. student at the University of Alberta under the supervision of J. A. W. Elliott, while the question was formulated based on S. Hejazi's Ph.D. work at Tarbiat Modares University under the supervision of H. Pahlavanzadeh. The visit was funded by a scholarship to S. Hejazi from the Ministry of Science, Research and Technology of Iran. J. A. W. Elliott holds a Canada Research Chair in Thermodynamics and acknowledges support from NSERC Discovery Grant RPGIN-2016-05502.

REFERENCES

(1) Vedantam, S.; Ranade, V. V. Crystallization: Key Thermodynamic, Kinetic and Hydrodynamic Aspects. *Sadhana* **2013**, *38*, 1287–1337.

(2) Sloan, E. D.; Koh, C. A. *Clathrate Hydrates of Natural Gases*, 3rd ed.; CRC Press: Boca Raton, FL, 2008.

(3) Shichiri, T.; Nagata, T. Effect of Electric Currents on the Nucleation of Ice Crystals in the Melt. *J. Cryst. Growth* **1981**, *54*, 207–210.

(4) Sun, W.; Chen, Z.; Huang, S. Effect of an External Electric Field on Liquid Water Using Molecular Dynamics Simulation with a Flexible Potential. *J. Shanghai Univ.* **2006**, *10*, 268–273.

(5) Braslavsky, I.; Lipson, S. G. Electrofreezing Effect and Nucleation of Ice Crystals in Free Growth Experiments. *Appl. Phys. Lett.* **1998**, *72*, 264–266.

(6) Choi, E. M.; Yoon, Y. H.; Lee, S.; Kang, H. Freezing Transition of Interfacial Water at Room Temperature Under Electric Fields. *Phys. Rev. Lett.* **2005**, *95*, 085701.

(7) Hozumi, T.; Saito, A.; Okawa, S.; Eshita, Y. Effects of Shapes of Electrodes on Freezing of Supercooled Water in Electric Freeze Control. *Int. J. Refrig.* **2005**, *28*, 389–395.

(8) Hozumi, T.; Saito, A.; Okawa, S.; Watanabe, K. Effects of Electrode Materials on Freezing of Supercooled Water in Electric Freeze Control. *Int. J. Refrig.* **2003**, *26*, 537–542.

(9) Xanthakis, E.; Le-Bail, A.; Havet, M. Freezing Combined with Electrical and Magnetic Disturbances. In *Emerging Technologies for Food Processing*, 2nd ed.; Academic Press: San Diego, 2014; pp 563–579..

(10) Xanthakis, E.; Havet, M.; Chevallier, S.; Abadie, J.; Le-Bail, A. Effect of Static Electric Field on Ice Crystal Size Reduction During Freezing of Pork Meat. *Innovative Food Sci. Emerging Technol.* **2013**, *20*, 115–120.

(11) Orlowska, M.; Havet, M.; Le-Bail, A. Controlled Ice Nucleation under High Voltage DC Electrostatic Field Conditions. *Food Res. Int.* **2009**, *42*, 879–884.

(12) Rau, W. Eiskeimbildung durch dielektrische Polarisation. *Z. Naturforsch., A: Phys. Sci.* **1951**, *6*, 649–657.

(13) Salt, R. W. Effect of Electrostatic Field on Freezing of Supercooled Water and Insects. *Science* **1961**, *133*, 458–459.

(14) Stan, C. A.; Tang, S. K. Y.; Bishop, K. J. M.; Whitesides, G. M. Externally Applied Electric Fields up to 1.6×10^5 V/M Do Not Affect the Homogeneous Nucleation of Ice in Supercooled Water. *J. Phys. Chem. B* **2011**, *115*, 1089–1097.

(15) Wei, S.; Xiaobin, X.; Hong, Z.; Chuanxiang, X. Effects of Dipole Polarization of Water Molecules on Ice Formation under an Electrostatic Field. *Cryobiology* **2008**, *56*, 93−99.
(16) Svishchev, I. M.; Kusalik, P. G. Electrofreezing of Liquid Water: A Microscopic Perspective. *J. Am. Chem. Soc.* **1996**, *118*, 649−654.
(17) Doolittle, J. B.; Vali, G. Heterogeneous Freezing Nucleation in Electric Fields. *J. Atmos. Sci.* **1975**, *32*, 375−379.
(18) Roulleau, M.; Evans, L.; Fukuta, N. The Electrical Nucleation of Ice in Supercooled Clouds. *J. Atmos. Sci.* **1971**, *28*, 737−740.
(19) Wilson, P. W.; Osterday, K.; Haymet, A. D. The Effects of Electric Field on Ice Nucleation May Be Masked by the Inherent Stochastic Nature of Nucleation. *CryoLetters* **2009**, *30*, 96−99.
(20) Conrad, H. Influence of an Electric or Magnetic Field on the Liquid−Solid Transformation in Materials and on the Microstructure of the Solid. *Mater. Sci. Eng., A* **2000**, *287*, 205−212.
(21) Bryskiewicz, T. In Quest of Unrestricted Growth of Bulk Crystals by Liquid Phase Electroepitaxy. *J. Cryst. Growth* **1995**, *153*, 19−24.
(22) Li, J.; Ma, J.; Gao, Y.; Zhai, Q. Research on Solidification Structure Refinement of Pure Aluminum by Electric Current Pulse with Parallel Electrodes. *Mater. Sci. Eng., A* **2008**, *490*, 452−456.
(23) Li, X.; Lu, F.; Cui, H.; Tang, X. Migration Behavior of Solidification Nuclei in Pure Al Melt under Effect of Electric Current Pulse. *Trans. Nonferrous Met. Soc. China* **2014**, *24*, 192−198.
(24) Petersen, A.; Rau, G.; Glasmacher, B. Reduction of Primary Freeze-Drying Time by Electric Field Induced Ice Nucleus Formation. *Heat Mass Transfer* **2006**, *42*, 929−938.
(25) Simura, R.; Nakamura, K.; Uda, S. Change of Melting Temperature of Non-Doped and Mg-Doped Lithium Niobate Under an External Electric Field. *J. Cryst. Growth* **2008**, *310*, 3873−3877.
(26) Uda, S.; Huang, X.; Koh, S. Transformation of The Incongruent-Melting State to The Congruent-Melting State Via an External Electric Field for The Growth of Langasite. *J. Cryst. Growth* **2005**, *281*, 481−491.
(27) Quan, X.; Chen, G.; Cheng, P. A Thermodynamic Analysis for Heterogeneous Boiling Nucleation Under an External Electric Field. *Int. J. Heat Mass Transfer* **2013**, *65*, 308−313.
(28) Jha, P. K.; Sadot, M.; Vino, S. A.; Jury, V.; Curet-Ploquin, S.; Rouaud, O.; Havet, M.; Le-Bail, A. A Review On Effect of DC Voltage On Crystallization Process in Food Systems. *Innovative Food Sci. Emerging Technol.* **2017**, *42*, 204−219.
(29) Acharya, P. V.; Bahadur, V. Fundamental Interfacial Mechanisms Underlying Electrofreezing. *Adv. Colloid Interface Sci.* **2018**, *251*, 26−43.
(30) Pahlavanzadeh, H.; Hejazi, S.; Manteghian, M. Hydrate Formation Under Static and Pulsed Electric Fields. *J. Nat. Gas Sci. Eng.* **2020**, *77*, 103232.
(31) Shardt, N.; Elliott, J. A. W. Gibbsian Thermodynamics of Cassie−Baxter Wetting (Were Cassie and Baxter Wrong? Revisited). *Langmuir* **2018**, *34*, 12191−12198.
(32) Shardt, N.; Elliott, J. A. W. Gibbsian Thermodynamics of Wenzel Wetting (Was Wenzel Wrong? Revisited). *Langmuir* **2020**, *36*, 435−446.
(33) Zargarzadeh, L.; Elliott, J. A. W. Bubble Formation in a Finite Cone: More Pieces to the Puzzle. *Langmuir* **2019**, *35*, 13216−13232.
(34) Ward, C. A.; Levart, E. Conditions for Stability of Bubble Nuclei in Solid Surfaces Contacting a Liquid−Gas Solution. *J. Appl. Phys.* **1984**, *56*, 491−500.
(35) Zargarzadeh, L.; Elliott, J. A. W. Comparative Surface Thermodynamic Analysis of New Fluid Phase Formation between a Sphere and a Flat Plate. *Langmuir* **2013**, *29*, 3610−3627.
(36) Zargarzadeh, L.; Elliott, J. A. W. Thermodynamics of Surface Nanobubbles. *Langmuir* **2016**, *32*, 11309−11320.
(37) Eslami, F.; Elliott, J. A. W. Thermodynamic Investigation of the Barrier for Heterogeneous Nucleation on a Fluid Surface in Comparison with a Rigid Surface. *J. Phys. Chem. B* **2011**, *115*, 10646−10653.
(38) Eslami, F.; Elliott, J. A. W. Design of Microdrop Concentrating Processes. *J. Phys. Chem. B* **2013**, *117*, 2205−2214.
(39) Eslami, F.; Elliott, J. A. W. Stability Analysis of Microdrops during Concentrating Processes. *J. Phys. Chem. B* **2014**, *118*, 3630−3641.
(40) Eslami, F.; Elliott, J. A. W. Role of Precipitating Solute Curvature on Microdrops and Nanodrops during Concentrating Processes: The Nonideal Ostwald−Freundlich Equation. *J. Phys. Chem. B* **2014**, *118*, 14675−14686.
(41) Voitcu, O.; Elliott, J. A. W. Equilibrium of Multi-Phase Systems in Gravitational Fields. *J. Phys. Chem. B* **2008**, *112* (38), 11981−11989.
(42) Shardt, N.; Elliott, J. A. W. Thermodynamic Study of the Role of Interface Curvature on Multicomponent Vapor−Liquid Phase Equilibrium. *J. Phys. Chem. A* **2016**, *120*, 2194−2200.
(43) Shardt, N.; Elliott, J. A. W. Isobaric Vapor−Liquid Phase Diagrams for Multicomponent Systems with Nanoscale Radii of Curvature. *J. Phys. Chem. B* **2018**, *122*, 2434−2447.
(44) Ashworth, E. N.; Abeles, F. B. Freezing Behavior of Water in Small Pores and the Possible Role in the Freezing of Plant Tissues. *Plant Physiol.* **1984**, *76*, 201−204.
(45) Mazur, P. The Role of Cell Membranes in the Freezing of Yeast and Other Single Cells. *Ann. N. Y. Acad. Sci.* **1965**, *125*, 658−676.
(46) Acker, J. P.; Elliott, J. A. W.; McGann, L. E. Intercellular Ice Propagation: Experimental Evidence for Ice Growth through Membrane Pores. *Biophys. J.* **2001**, *81*, 1389−1397.
(47) Liu, F.; Zargarzadeh, L.; Chung, H. J.; Elliott, J. A. W. Thermodynamic Investigation of the Effect of Interface Curvature on the Solid−Liquid Equilibrium and Eutectic Point of Binary Mixtures. *J. Phys. Chem. B* **2017**, *121*, 9452−9462.
(48) Hayt, W. H.; Buck, J. A. *Engineering Electromagnetics*, 3rd ed.; Springer International Publishing: 2015.
(49) Cheng, D. K. *Field and Wave Electromagnetic*, 2nd ed.; Addison-Wesley Publishing Co.: 1983.
(50) Callen, H. B. *Thermodynamics and an Introduction to Thermostatistics*, 2nd ed.; John Wiley & Sons: New York, 1985.
(51) Gibbs, J. W. On the Equilibrium of Heterogeneous Substances. *Transactions of the Connecticut Academy of Arts and Sciences* **1876**, *3*, 108−248; *Transactions of the Connecticut Academy of Arts and Sciences* **1878**, *3*, 343−524. Republished as: Gibbs, J. W. *The Scientific Papers of J. Willard Gibbs*; Ox Bow: Woodbridge, CT, 1993; Vol. *1*, pp 5−353.
(52) Polyanin, A. D; Manzhirov, A. V. *Mathematics for Engineers and Scientists*; Chapman & Hall: 2006.
(53) Ozerov, R. P.; Vorobyev, A. A. Dielectric Properties of Substances. In *Physics for Chemists*; Elsevier: 2007.
(54) Duan, C.; Majumdar, A. Anomalous Ion Transport in 2-nm Hydrophilic Nanochannels. *Nat. Nanotechnol.* **2010**, *5*, 848−852.
(55) Persson, F.; Tegenfeldt, J. O. DNA in Nanochannels—Directly Visualizing Genomic Information. *Chem. Soc. Rev.* **2010**, *39*, 985.
(56) Levy, S. L.; Craighead, H. G. DNA Manipulation, Sorting, And Mapping in Nanofluidic Systems. *Chem. Soc. Rev.* **2010**, *39*, 1133.
(57) Tsukahara, T.; Hibara, A.; Ikeda, Y.; Kitamori, T. NMR Study of Water Molecules Confined in Extended Nanospaces. *Angew. Chem., Int. Ed.* **2007**, *46*, 1180.
(58) Hiemstra, T.; Van Riemsdijk, W. H. Physical Chemical Interpretation of Primary Charging Behaviour of Metal (Hydr) Oxides. *Colloids Surf.* **1991**, *59*, 7−25.
(59) Hibara, A.; Saito, T.; Kim, H.; Tokeshi, M.; Ooi, T.; Nakao, M.; Kitamori, T. Nanochannels on a Fused-Silica Microchip and Liquid Properties Investigation by Time-Resolved Fluorescence Measurements. *Anal. Chem.* **2002**, *74*, 6170−6176.
(60) Fumagalli, L.; Esfandiar, A.; Fabregas, R.; Hu, S.; Ares, P.; Janardanan, A.; Yang, Q.; Radha, B.; Taniguchi, T.; Watanabe, K.; et al. Anomalously Low Dielectric Constant of Confined Water. *Science* **2018**, *360*, 1339−1342.
(61) Buckingham, A. D. Theory of The Dielectric Constant at High Field Strengths. *J. Chem. Phys.* **1956**, *25*, 428.

https://dx.doi.org/10.1021/acs.jpcb.0c08754
J. Phys. Chem. B 2021, 125, 1271−1281

(62) Yeh, I.-C.; Berkowitz, M. L. Dielectric Constant of Water at High Electric Fields: Molecular Dynamics Study. *J. Chem. Phys.* **1999**, *110*, 7935.
(63) Appleby, A. J. Electron Transfer Reactions with and without Ion Transfer. In *Modern Aspects of Electrochemistry*; Conway, B. E., Vayenas, C. G., White, R. E., Gamboa-Adelco, M. E., Eds.; Plenum Publishers: New York, NY, 2005; Vol. *38*, p 175..
(64) Booth, F. The Dielectric Constant of Water and The Saturation Effect. *J. Chem. Phys.* **1951**, *19*, 391.
(65) Booth, F. Dielectric Constant of Polar Liquids at High Field Strengths. *J. Chem. Phys.* **1955**, *23*, 453.
(66) Rawle, A. F. Refractive Index Measurements. *Encyclopedia of Spectroscopy and Spectrometry*, 3rd ed.; Academic Press: 2017.
(67) *CRC Handbook of Chemistry and Physics*, 56th ed.; Weast, R. C., Ed.; CRC Press: 1975.
(68) Cheng, K. J.; Chaddock, J. B. Deformation and Stability of Drops and Bubbles in an Electric Field. *Phys. Lett. A* **1984**, *106*, 51−53.
(69) *CRC Handbook of Chemistry and Physics*, 85th ed.; Lide, D. R., Ed.; CRC Press: 2004.
(70) Lane, L. B. Freezing Points of Glycerol and Its Aqueous Solutions. *Ind. Eng. Chem.* **1925**, *17*, 924.

https://dx.doi.org/10.1021/acs.jpcb.0c08754
J. Phys. Chem. B 2021, 125, 1271−1281